Author Manuscript

Author Manuscript

Author Manuscript

Author Manuscript

HHS Public Access

Author manuscript

J Magn Reson Imaging. Author manuscript; available in PMC 2017 January 03.

Published in final edited form as:

J Magn Reson Imaging. 2010 March ; 31(3): 589–600. doi:10.1002/jmri.22081.

Diagnosis of Cirrhosis With Intravoxel Incoherent Motion Diffusion MRI and Dynamic Contrast-Enhanced MRI Alone and in Combination: Preliminary Experience

Jignesh Patel, MD, **Eric E. Sigmund, PhD**, **Henry Rusinek, PhD**, **Marcel Oei, MD**, **James S. Babb, PhD**, and **Bachir Taouli, MD***

NYU Langone Medical Center, Department of Radiology, New York, New York, USA.

Abstract

Purpose—To report our preliminary experience with the use of intravoxel incoherent motion (IVIM) diffusion-weighted magnetic resonance imaging (DW-MRI) and dynamic contrast-enhanced (DCE)-MRI alone and in combination for the diagnosis of liver cirrhosis.

Materials and Methods—Thirty subjects (16 with noncirrhotic liver, 14 with cirrhosis) were prospectively assessed with IVIM DW-MRI ($n = 27$) and DCE-MRI ($n = 20$). IVIM parameters included perfusion fraction (PF), pseudodiffusion coefficient (D*), true diffusion coefficient (D), and apparent diffusion coefficient (ADC). Model-free DCE-MR parameters included time to peak (TTP), upslope, and initial area under the curve at 60 seconds (IAUC60). A dual input single compartmental perfusion model yielded arterial flow (Fa), portal venous flow (Fp), arterial fraction (ART), mean transit time (MTT), and distribution volume (DV). The diagnostic performances for diagnosis of cirrhosis were evaluated for each modality alone and in combination using logistic regression and receiver operating characteristic analyses. IVIM and DCE-MR parameters were compared using a generalized estimating equations model.

Results—PF, D*, D, and ADC values were significantly lower in cirrhosis ($P = 0.0056$–0.0377), whereas TTP, DV, and MTT were significantly increased in cirrhosis ($P = 0.0006$–0.0154). There was no correlation between IVIM- and DCE-MRI parameters. The highest Az (areas under the curves) values were observed for ADC (0.808) and TTP-DV (0.952 for each). The combination of ADC with DV and TTP provided 84.6% sensitivity and 100% specificity for diagnosis of cirrhosis.

Conclusion—The combination of DW-MRI and DCE-MRI provides an accurate diagnosis of cirrhosis.

Keywords

diffusion-weighted MRI; dynamic contrast-enhanced MRI; liver; cirrhosis

*Address reprint requests to: B.T., Department of Radiology, Mount Sinai Medical Center, One Gustave Levy Place, Box 1234, New York, NY 10029. bachir.taouli@mountsinai.org.

Presented at the 2009 ISMRM meeting.

Author Manuscript Author Manuscript Author Manuscript Author Manuscript

NONINVASIVE DIAGNOSIS of liver fibrosis and cirrhosis in patients with chronic liver disease is critical, as cirrhotic patients are at higher risk of endstage liver disease, portal hypertension, and hepatocellular carcinoma (HCC) (1). In addition, cirrhotic patients with chronic viral hepatitis are less likely to respond to antiviral therapy (2,3).

Magnetic resonance imaging (MRI) is a promising method for assessment of diffuse liver disease, given the potential for multiparametric information. In vivo metrics obtained with both diffusion-weighted (DW) MRI (4–14) and dynamic contrast-enhanced (DCE) MRI (15,16) have been shown to represent potential markers of fibrosis and cirrhosis. The mechanism of perfusion changes in liver fibrosis are better understood than changes observed with DW-MRI. Depending on the acquisition parameters, apparent diffusion coefficient (ADC; $\times 10^{-3}$ mm^2/s) is known to reflect variable combinations of diffusion and perfusion effects. The concept of IVIM (intravoxel incoherent motion)—initially described by Le Bihan et al (17–20) in brain imaging—has the potential to measure both true molecular diffusion and incoherent motion of water molecules in the capillary network, known as pseudodiffusion. Because cirrhosis involves accumulation of extracellular matrix that may affect both true diffusion and microcirculation, IVIM DW-MRI should be sensitive to cirrhotic changes. However, the IVIM model has been rarely described in the liver (21–23). Yamada et al (21) were the first to assess IVIM DWMRI in abdominal organs, although they used only a limited number of b-values (30, 300, 900, and 1100 s/mm^2), and did not calculate pseudodiffusion values (D* values; $\times 10^{-3}$ mm^2/s). Recently, Luciani et al (23) demonstrated lower ADC and D* values in cirrhotic versus normal livers without differences in D (true diffusion coefficient; $\times 10^{-3}$ mm^2/s) and PF (perfusion fraction). There are no published reports on the comparison and combination of DW- and DCE-MRI to diagnose liver fibrosis or cirrhosis.

The purpose of our study was to report our preliminary experience with the use of IVIM DW-MRI and DCE-MRI alone and in combination for the diagnosis of liver cirrhosis.

MATERIALS AND METHODS

Study Design and Patient Population

This was a Health Insurance Portability and Accountability Act (HIPAA)-compliant prospective study that was approved by our local Institutional Review Board. Informed signed consent was obtained from all subjects. Thirty subjects (M/F 18/12, mean age 48 years, range 23–89 years) were prospectively enrolled from July 2008 to March 2009. The subjects were stratified as noncirrhotic ($n = 16$) or cirrhotic ($n = 14$) based on clinical history, liver function tests, MRI findings, and pathologic data.

The noncirrhotic group included the following subjects: nine healthy volunteers (M/F 8/1, mean age 30 years, range 23–43 years) without history of chronic liver disease or significant alcohol intake, assessed only with IVIM DW-MRI. Six patients (M/F 0/6, mean age 45 years, range 23–70 years) without a history of chronic liver disease or significant alcohol intake and with normal liver function tests, evaluated for benign liver lesions (hemangiomas, adenomas, or focal nodular hyperplasia). A 35-year-old female patient with periportal fibrosis of unknown etiology (diagnosed with partial hepatectomy for an indeterminate liver

Author Manuscript Author Manuscript Author Manuscript Author Manuscript

lesion). The cirrhotic group included 14 patients (M/F 10/4, mean age 62 years, range 26–89 years) with a history of chronic liver disease. Cirrhosis was proven by histopathology ($n = 3$) or MRI findings showing liver nodularity and portal hypertension ($n = 11$). Cirrhosis was attributed to chronic hepatitis C ($n = 9$), alcohol intake ($n = 3$), or autoimmune hepatitis ($n = 2$). Four of these patients had focal lesions consistent with HCC. A total of 17 patients (four noncirrhotic and 13 cirrhotic) underwent both IVIM and DCE-MRI.

IVIM DW-MRI

MRI was performed using one of three 1.5 T systems (Magnetom Avanto, Symphony and Sonata, Siemens Healthcare, Erlangen, Germany). IVIM DW-MRI was acquired before any contrast administration in 27 subjects (three patients had only DCE-MRI without DW-MRI), using free breathing or navigator-echo triggered (PACE: prospective acquisition correction, Siemens Healthcare) (24) single-shot echoplanar imaging (SS EPI) acquisition (parameters in Table 1). PACE and free-breathing acquisitions were performed in 21 and 10 subjects, respectively (four volunteers had both PACE and free-breathing acquisitions performed). Coronal over transverse acquisition was chosen to match the coronal acquisition used with DCEMRI.

DCE-MRI

DCE-MRI was performed in 20 patients (nine healthy volunteers and one patient with renal insufficiency did not have contrast injection). Perfusion imaging of the whole liver was performed using a 3D interpolated spoiled gradient-recalled echo sequence in the coronal plane. Patients fasted for 6 hours before the study. The arms were elevated to minimize aliasing artifacts. Three acquisitions were performed before contrast injection, and the first postcontrast acquisition started at the end of the injection of 10 mL of gadobenate dimeglumine (MultiHance, Bracco Diagnostics, Princeton, NJ) followed by a 20-mL saline flush injected at 5 mL/sec using an MR-compatible power injector (Spectris, Medrad, Indianola, PA). Fifty coronal volumetric acquisitions images were acquired every 3.5–5 seconds for ≈3–4 minutes (parameters in Table 1). Patients were instructed to suspend respiration at end expiration (in order to minimize misregistration) during all acquisitions, with the first breath hold lasting ≈25–30 seconds and subsequent free shallow breathing. The rationale of coronal plane imaging was to minimize flow-related enhancement of the aorta (25). IVIM DW-MRI and DCE-MRI were incorporated into the routine MRI protocol and added ≈10 minutes to the total imaging time.

Image Analysis

MR images were assessed by three observers (observer 1, who was a body MRI fellow; observer 2, who was a medical student; and observer 3, a radiologist with 5 years experience in body MRI).

IVIM DW-MRI Analysis

ROI (region of interest) placement: All ROIs were manually positioned by observers 1 and 2 in consensus on SS EPI diffusion images on a commercial workstation (Syngo, Siemens Healthcare) for all b-values. A large ROI (2–3 cm) was positioned in the right hepatic lobe

Author Manuscript Author Manuscript Author Manuscript Author Manuscript

on three consecutive slices centered on the main portal vein (Fig. 1). ROIs were placed away from lesions, confluent fibrosis, and large intrahepatic vessels. The left hepatic lobe was excluded due to potential cardiac motion artifacts that may artificially increase values of IVIM parameters. Mean signal intensity (SI) was measured within each ROI, and values of three ROIs (from three slices) were averaged for biexponential fitting (see below).

In addition, for each slice position an ROI was placed over air for b = 1000 s/mm^2 images. This value was compared to SI of the right hepatic lobe as detailed above. All slice positions or entire datasets were excluded when the ratio of the liver signal intensity to that in the air ROI (defined here as signal-to-noise ratio, SNR) was less than 2 and thus were potentially biased by Rician noise (26).

Segmented biexponential fitting (Fig. 2): The fitting was performed by an expert observer (observer 4, with 12 years experience in DW-MRI) to derive PF, D, D*, and ADC. The values obtained on a per-patient basis were calculated by averaging the three ROI measurements.

The IVIM concept (17) is based on the assumption that water molecules in a voxel can be separated into two compartments, ie, an intravascular component with volume fraction PF, representing the water molecules flowing in the pseudorandom oriented capillary network (pseudodiffusion coefficient, D*) and the extravascular component with volume fraction 1-PF, showing passive, restricted diffusion (D). When the MR signal is measured with a sufficient number of different diffusion-weighting factors (b-values), the two compartments can be identified and characterized as described below:

$$S_b/S_o = (1 - PF)\exp(-bD) + PF\exp(-bD^*) \quad [1]$$

Since a simultaneous nonlinear fit for all parameters in Eq. [1] can be problematic in cases of low perfusion fraction, limited sampling, or low precision (27), a more stable "segmented" analysis procedure was adopted as follows, and as employed in other reports (28–30). Typically, D* is significantly greater than D (17) by a factor of ≈10, so that when b value is greater than 200 s/mm^2, the influence of the pseudodiffusion term on the signal decay is quite small. Thus, in the higher b-value regime, Eq. [1] can then be simplified into a linear fit equation whereby D can be estimated:

$$S_b = \mathrm{S}_{int}\exp(-bD) \quad [2]$$

Here S_{int} is the b = 0 intercept of the high b-value exponential fit, which allows the perfusion fraction to be estimated according to:

$$PF = (\mathrm{S}_0 - \mathrm{S}_{\mathrm{int}})/\mathrm{S}_0 \quad [3]$$

With D and PF values determined by using Eq. [2], D* values can be calculated by using a partially constrained nonlinear regression algorithm based on Eq. [1].

Author Manuscript Author Manuscript Author Manuscript Author Manuscript

The ADC was obtained by using all b-values (0–1000 s/mm^2) and then fitted to the equation:

$$S_b = S_0 \exp(-b \ ADC) \quad [4]$$

All regression algorithms and parametric map generation of the parameters PF, D, D*, and ADC were performed with custom-written code written in IgorPro software (Wavemetrics, Lake Oswego, OR). The above algorithm was employed primarily for the DW-MRI ROI analysis, from which all quantitative metrics were derived for correlation with other data. The same procedure was applied on a voxelwise basis to select normal and cirrhotic cases for pure qualitative illustration, since the SNR per voxel is significantly less than that of the large ROI analysis.

Assessment of Reproducibility of IVIM Parameters—Test/retest evaluation was performed to assess reproducibility by repeating IVIM DWI in the same subjects within a 1–2 week time period on the same MR unit without any intervention in the interval. IVIM DW-MRI was repeated in five subjects (one patient with noncirrhotic liver and four volunteers) using PACE ($n = 5$) and free breathing acquisitions ($n = 4$).

DCE-MRI Analysis

ROI placement: The images were transferred to a PC for analysis. Home-grown software was used for analysis (Firevoxel). To determine the vascular input functions (VIF), ROIs were manually drawn on the main portal vein (at the level of the porta hepatis) and proximal abdominal aorta (at the level of the celiac axis, used as a surrogate of the hepatic artery). ROIs for the portal vein were drawn for each timeframe to correct for spatial misregistration due to respiratory motion. In addition, six liver ROIs (measuring 2–3 cm, 3 in the right lobe and 3 in the left lobe) were placed by observers 2 and 3 in consensus. Large vascular structures or liver lesions were avoided.

Model-free perfusion parameters: All perfusion computations were performed by an expert observer (observer 5, with 20 years in perfusion modeling and image processing). For each liver region three parameters (TTP [time to peak], upslope, and IAUC60 [area under the curve at 60 sec]) were defined using simplified, model-free computations that did not require information about arterial or portal vein input functions. From each signal activity curve S(t) the values of rise time t_{rise} and peak time t_{peak} were identified. The value t_{rise} was defined as the earliest sample with signal exceeding the baseline threshold:

$$M_0 + 2\sigma_0 \quad [5]$$

where M_0 was the mean value M_0 and σ_0 the standard deviation of the signal measured during the first five (ie, preinjection) acquisitions. The value t_{peak} was the timepoint at which S(t) reached its maximum. These timepoints t_{rise} and t_{peak} served to define TTP, peak concentration c_{max}, and average upslope U according to:

Author Manuscript Author Manuscript Author Manuscript Author Manuscript

$$TTP = t_{peak} - t_{rise} \quad [6]$$

$$c_{max} = C(t_{peak}) \quad [7]$$

$$U = C(t_{peak})/TTP \quad [8]$$

C(t) in the above equation denotes the concentration-versus-time curve derived from S(t). In addition, the area under the time activity curve of gadolinium contrast over 60 seconds from the start of contrast enhancement was quantified (IAUC60).

Perfusion modeling: SI measurements were normalized by subtracting the SI value of the initial unenhanced image from the SI measurements of the subsequent enhanced images, then dividing the difference by the initial SI value. SI curves were then obtained from all ROI data (Fig. 3). A linear relationship was assumed between SI and gadolinium concentration for the range of expected concentrations in the liver (0.0–0.5 mM/L) and blood (0–5 mM/L). Our conversion was therefore based on the approximation: $c = k(S - S_0)/S_0$ (31), in which S_0 is precontrast SI, S is postcontrast SI, and k the scaling constant (0.395 for liver and 0.201 for blood). These constants are based on prior phantom and human calibration study (32). The resulting time–activity curves were fitted using a dual-input single compartmental model which was validated previously (15,16,33). This model reflects the dual blood supply from the portal vein and hepatic artery received by the liver. The general equation for the dual-input kinetic model is:

$$C_L(t) = \int_0^t \left[k_{1a}C_a\left(t' - \delta\right) + k_{1p}C_p\left(t'\right)\right] e^{-k_2\left(t-t'\right)} dt' \quad [9]$$

where $C_a(t)$, $C_p(t)$, and $C_L(t)$ represent the concentrations of the contrast in the aorta, the portal vein, and the liver, respectively; δ represents the transit times from the aorta region to the liver region of interest, k_{1a} represents the aortic inflow rate constant, k_{1p} the portal venous inflow rate constant, and k_2 the outflow rate constant. A fitting procedure was performed to determine k_{1a}, k_{1p}, k_2, and δ using locally developed software written in C++. The distribution volume (DV in %) of Gd-contrast through the liver compartment was calculated as DV = 100 (k_{1a} + k_{1p})/k_2, and mean transit time (MTT in sec) as 1/k_2. MTT is the average time it takes a Gd molecule to traverse the liver from arterial/portal entry to venous exit. Inflow constants k_{1a}, k_{1p}, were converted to arterial and portal flow rates F_a (arterial liver blood flow), F_p (portal liver blood flow), both expressed in ml/100g/min, and then used to compute the total flow ($F_a + F_p$) as well as the arterial fraction (ART, in %) = $100 \times F_a/(F_a + F_p)$.

Author Manuscript Author Manuscript Author Manuscript Author Manuscript

Statistical Analysis

SAS v. 9.0 (Cary, NC) was used for statistical computations. All statistical analyses employed result from ROI analysis. An exact Mann–Whitney test was used to compare cirrhotic and noncirrhotic subjects in terms of each imaging measure. Binary logistic regression was used to derive models to predict cirrhosis using sets of two or more imaging measures. Receiver operating characteristic (ROC) curve analysis was used to identify cutoff values for the imaging measures that maximized the average of sensitivity and specificity when the threshold was used to define patients as test positive or test negative for cirrhosis. A generalized estimating equations (GEE) model was used to compare sensitivity and specificity of IVIM and DCE-MRI parameters. All reported P values are two-sided. Each of PF and D* were correlated with DCE-MR parameters using the Pearson correlation test. Statistical significance was defined as $P < 0.05$. Reproducibility of imaging parameters was evaluated using coefficient of variation (CV = SD/mean of 2 measures) analysis.

RESULTS

IVIM DW-MRI Parameters (Table 2)

ROI analysis results showed that ADC values were significantly higher than D values in both the noncirrhotic and cirrhotic subjects ($P = 0.001$ and 0.002, respectively), confirming the perfusion effect on ADC values. All IVIM parameters (ADC, D*, D, PF) were significantly reduced in the cirrhotic group compared to the noncirrhotic group ($P = 0.0071$-0.0392) (Table 2, Figs. 2, 4). The most significant difference was observed for ADC. The relationships shown in Table 2 and Figure 4, derived from robust large ROI analysis, are qualitatively consistent with example parametric maps of IVIM parameters in a normal and cirrhotic patient (Fig. 5). Although spatial textures are complex, the mean values of each IVIM parameter across the liver are lower in the cirrhotic versus normal patient.

Reproducibility of IVIM parameters (in the subset of patients in whom repeat PACE or free-breathing DWI was performed) was excellent for ADC and D, good for PF, and fair for D* (Table 3). Reproducibility was higher with the navigator triggered acquisition.

DCE-MRI Parameters (Table 4)

TTP, DV, and MTT were all significantly increased in the cirrhotic group when compared to the noncirrhotic group ($P = 0.002$–0.0187) (Table 4, Figs. 3, 6). F_a and ART were increased, whereas upslope and IAUC60 were decreased in cirrhosis, with a trend toward significance ($P = 0.0791$–0.0913), likely due to sample size. Portal venous flow (F_p) and total liver flow ($F_a + F_p$) were decreased in cirrhosis without reaching significance.

Correlation Between IVIM and DCE-MRI Parameters

There was no significant correlation between each of PF and D* with DCE-MR parameters (Pearson correlation coefficients ranging from −0.35 to 0.40; $P > 0.14$, Table 5).

Diagnostic Performance of IVIM DW- and DCE-MRI Alone and in Combination (Table 6)

Stepwise variable selection in the context of logistic regression identified ADC as the best predictor of cirrhosis from among the IVIM measures (Az 0.808, sensitivity 84.6%,

Author Manuscript Author Manuscript Author Manuscript Author Manuscript

specificity 71.4%). The stepwise variable selection identified DV and TTP as the best predictors of cirrhosis from among the DCE measures (Az 0.952, sensitivity 85.7%, specificity 100.0% for both) followed by MTT (Az 0.845, sensitivity 100.0%, specificity 83.3%), and IAUC60 (Az 0.804, sensitivity 85.7%, specificity 75.0%).

The Az of DV and TTP were higher than that of ADC; however, the comparison between IVIM and DCE-MR parameters using the GEE model showed no significant difference (P = 0.9281 for sensitivity and 1.0 for specificity).

In the 17 patients who had both IVIM DW- and DCE-MRI, the combination of ADC with TTP and DV provided 84.6% sensitivity (11/13), 100% specificity (4/4), 100% positive predictive value (11/11), 66.6% negative predictive value (4/6), and 88.2% (15/17) accuracy for diagnosing cirrhosis (Fig. 7). All four noncirrhotic patients had decreased TTP and DV, and the 11/13 cirrhotic patients had decreased ADC and increased TTP or increased DV.

DISCUSSION

In our study we demonstrated altered IVIM (ADC, PF, D*, and D) and DCE-MR parameters (TTP, DV, and MTT) in liver cirrhosis, with excellent diagnostic accuracy for diagnosing cirrhosis using ADC and TTP-DV. In addition, we showed that the combination of ADC with TTP and DV yielded 84.6% sensitivity and 100% specificity for diagnosing cirrhosis. To our knowledge, this is the first study reporting the use of combined IVIM and DCE-MR acquisitions in liver imaging.

Patients with chronic hepatitis (including mostly viral, alcoholic, and nonalcoholic steatohepatitis) are at high risk of developing liver fibrosis and cirrhosis (1). Accurate diagnosis of liver cirrhosis is critical, as cirrhotic patients are at higher risk of endstage liver disease, portal hypertension, and HCC. The degree of fibrosis is commonly determined from liver biopsy, used to assess prognosis and guide therapy (34). However, liver biopsy is relatively invasive, expensive, limited by sample size, and difficult to repeat (35–40). Thus, noninvasive tools to assess the degree of injury and fibrosis of the whole liver are urgently needed.

DW-MRI (4–14) and DCE CT or MRI (15,16,33,41) parameters have been shown to be potentially useful for detection of liver fibrosis and cirrhosis, with a reported range of areas under the curve of 0.896–0.93 (11–13) for diagnosis of advanced fibrosis or cirrhosis. Most of these diffusion studies showing decreased liver ADC in cirrhosis (4–9, 13) or fibrosis (10–12, 14) compared to normal liver or mild degrees of fibrosis have quantified diffusion using a monoexponential fit, and have assumed pure diffusion restriction in relation with extracellular matrix accumulation. However, our findings and those from other investigators (21,23,42) suggest that both pure molecular diffusion and capillary perfusion contribute to signal attenuation in liver diffusion imaging. This is primarily attributed to the IVIM effect observed with the use of b-values <200 s/mm^2. The IVIM model—initially described in the brain by Le Bihan et al (17)—can discriminate true molecular diffusion from capillary perfusion (or pseudodiffusion). There is a paucity of data on the use of IVIM DW-MRI in the liver (21–23). Yamada et al (21) were the first to assess IVIM DW-MRI in abdominal

Author Manuscript Author Manuscript Author Manuscript Author Manuscript

organs. They reported PF, D, and ADC values in abdominal organs, but did not report D* values. They demonstrated lower D values compared to ADC values in abdominal organs and liver lesions (for example, average D, PF, and ADC values of normal liver were 0.76 × 10^{-3} mm^2/s, 29% and 0.87 × 10^{-3} mm^2/s, respectively). They showed no difference between normal and cirrhotic liver using any of the IVIM parameters. This may be attributed to the limited number of b-values used (30, 300, 900, and 1,100 s/mm^2), especially below 200 s/mm^2, which may limit the fitting precision. In addition, the relatively long TE used (123 msec) and lack of parallel imaging acquisition could both decrease SNR and the accuracy of diffusion coefficients (43). Moteki et al (22) evaluated 78 patients (with normal and cirrhotic livers) using SS EPI with b-values of 3, 50, 300 s/mm^2. They calculated only D and D* values, and found significantly lower D* values in cirrhosis compared to noncirrhotic liver (1.74 ± 2.51 vs. 6.68 ± 3.49 × 10^{-3} mm^2/s), with no difference in D values (1.29 ± 0.62 vs. 1.16 ± 0.69 × 10^{-3} mm^2/s). Their results were limited by the number and magnitude of b-values used. Moreover, ADC and PF values were not reported. Recently, Luciani et al (23) assessed 37 patients (12 cirrhotics and 25 with normal liver) with respiratory gated (using pneumatic belt) IVIM DW-MRI with 10 b-values (0, 10, 20, 30, 50, 80, 100, 200, 400, and 800 s/mm^2). They also demonstrated lower D values compared to ADC values in both patient populations, as shown in our study and the study by Yamada et al (21), and decreased ADC and D* in cirrhosis (mean ADC-D* in cirrhosis: 1.23 ± 0.4 and 59.4 ± 20.0 × 10^{-3} mm^2/s, compared to 1.39 ± 0.2 and 79.1 ± 18.1 × 10^{-3} mm^2/s in normal liver). However, D and PF were not different between the two patient populations (mean D and PF in cirrhosis: 1.19 ± 0.5 × 10^{-3} mm^2/s and 30.0 ± 5.7, compared to 1.10 ± 0.7 × 10^{-3} mm^2/s and 27.0 ± 5.3 in normal liver). The reason for discrepancy in the results between the study by Luciani et al (23) and our study is unclear, and may be related to the population and sequence parameters selected. The magnitude of differences in IVIM parameters between the two studies are present for ADC and to a larger extent for D* (mean for normal liver in Luciani et al: 79.1, compared to 39.61 in our study, mean for cirrhotic liver 59.4 vs. 27.89 × 10^{-3} mm^2/s). The differences in D* values could in part be accounted for by the higher number of b-values below 200 s/mm^2 utilized in their study (0, 10, 20, 30, 40, 50, 100, and 200 s/mm^2) compared to ours (0, 50, 100, 150, and 200 s/mm^2). Large differences in D* may also be attributed to fitting errors, as this parameter typically displays the largest fitting uncertainty in IVIM studies. Our results suggest that PF is lower in the cirrhotic group than in the noncirrhotic group, and our data support the theory that differences in total ADC between noncirrhotic and cirrhotic patients has a significant perfusional component but restriction of Brownian motion still plays a role at higher b-values. In our study, ADC was still the best IVIM parameter in terms of accuracy, with the best reproducibility, likely due to increased data points (including low and large b-values).

Previous reports have shown that advanced fibrosis and cirrhosis lead to reduced portal venous flow and increased arterial flow (known as the arterial buffer response) (44), as well as increased MTT and DV measured with DCE CT or MRI (15,16,33,41). A recent study has showed that DV was the best predictive parameter for diagnosing advanced fibrosis and cirrhosis (Az of 0.824, sensitivity of 76.9%, and specificity of 78.5% for DV ≥ 21.05%) (16). The current study showed higher Az for DV and MTT compared to the prior study by Hagiwara et al (16), which likely relates to a different patient selection (intermediate stages

Author Manuscript Author Manuscript Author Manuscript Author Manuscript

of fibrosis were not included in the current study). Model-free DCE-MR parameters have never been described before for the diagnosis of liver cirrhosis, and these may have a role in future studies, as these parameters are easy to quantify, without the need for vascular input function.

The relationship between perfusion parameters measured with IVIM versus those measured with DCE-MRI is unclear. In an opinion article, Le Bihan and Turner (45) suggested that the combination of PF and D* may potentially provide useful data for micro-circulation physiology (PF measures the fractional volume of capillary blood flowing in each voxel, and D* is proportional to the mean capillary segment length and to average blood velocity). They also suggested that CBF (cerebral blood flow) is directly proportional to the product PF × D*. In a contradictive opinion article, Henkelman (46) suggested that IVIM does not measure tissue perfusion as does DCE-MRI, as it is more sensitive to blood volume transit through a voxel. Data corroborating or contradicting these opinions is sparse, even in neuroimaging. For example, Wirestam et al (30) correlated brain IVIM parameters with dynamic susceptibility-contrast (DSC) MRI (calculating cerebral blood volume and flow, CBV and CBF) in 28 volunteers. They demonstrated a moderate significant correlation between PF and CBV ($r = 0.56$, $P < 0.001$) using asymptotic fitting (ie, segmented analysis). A key point in the comparison of IVIM and DCE or DSC MRI techniques is the effect of compartmental exchange. The evolution time of the DW-MRI sequence (≈100 msec) is insufficient for significant water exchange and thus the signal can be interpreted as separate intra- and extravascular compartments, with the parameters PF and D* referring to the intravascular compartment. Conversely, DCE-MRI tracks contrast continuously over much longer periods (several minutes) and thus necessarily involves intravascular, extravascular, and exchange dynamics. Correspondingly, of the parameters of the DCE-MRI model, eg, those reported in this study, none exclusively reflect microvascular volume or flow, but instead some composite encompassing total tracer transit. DSC MRI, on the other hand, employs susceptibility contrast on short timescales and, particularly for vasculature with a blood–brain barrier, also provides access to purely intravascular parameters (eg, CBF and CBV), motivating the aforementioned comparison of IVIM and DSC-MRI metrics. Indeed, since “perfusion” usually connotes not only vascularity but also the extravasation of blood products to surrounding parenchyma, the terms “perfusion fraction” or “perfusion-induced pseudodiffusion” can be misleading. While the terms historically arose to differentiate vascular from parenchymal effects in DW-MRI, care must be taken in attempts to reconcile them with DCE-MRI, which has distinctly different biophysical sensitivity. Finally, other effects unique to hepatic tissue may confound the association of IVIM exclusively with perfusive vascularity, including fast flow of bile ducts and venous drainage.

Based on this perspective and the current study results, we can confidently suggest that liver perfusion measurements with IVIM are not equivalent to perfusion parameters obtained with DCE-MRI, with no correlations observed. Therefore, we do not believe that IVIM can be used as a surrogate for DCE-MR perfusion. Since the parameters measured with each method do not relate, it is very attractive to combine the two methods for improved diagnostic accuracy, as shown in our patient population. This could be further assessed for prospective detection of intermediate stages of fibrosis.

Author Manuscript Author Manuscript Author Manuscript Author Manuscript

An important issue with DW- and DCE-MRI is reproducibility. Moteki and Horikoshi (22) reported a large variability of D and D* values with CV of 25.4% and 28.2% for D and D* values (measured on a single volunteer 11 times); however, their study was limited by the number of b-values used (3, 50, 300 s/mm^2), and they did not report CV of ADC and PF. A recent study on volunteers showed mean CV of 12.8% for liver ADC measurement using free-breathing DW-MRI (47). More recently, Koh et al (48) found better reproducibility of ADC total (using all b-values: 0, 50, 100, 250, 500, and 750 s/mm^2) and ADC high (using 100, 250, 500, and 750 s/mm^2), compared to ADC low (using 0, 50, and 100 s/mm^2). In our study we found good to excellent reproducibility of ADC, D, and PF, especially with the navigator triggered acquisition (CV <6% for ADC and D, and <12% for PF). D* had the worse reproducibility (with CV of 14.6% and 39.1% for navigator triggered and free breathing acquisitions, respectively). Regarding reproducibility of liver perfusion measurements, Miyazaki et al (49) recently reported excellent reproducibility of hepatic perfusion index (a semiquantitative perfusion parameter) measured in patients treated with an antiangiogenic compound.

We did not measure reproducibility of DCE-MR parameters in our study, and this could be assessed in a separate study.

Our study had several limitations. The ability to recruit noncirrhotic patients prospectively for the DCE-MRI portion of study was limited and as a result only four patients were included in this portion of the study. In the cirrhotic group, histopathologic confirmation was only available for three patients. Furthermore, we did not assess intermediate stages of fibrosis in this evaluation. One patient included in our noncirrhotic group was found to have heterogeneous areas of periportal fibrosis on pathology and this may have negatively skewed our results. Future studies assessing different stages of fibrosis using IVIM and DCE-MR parameters may be conducted. In our initial experience, only five b-values less than or equal to 200 s/mm^2 were implemented. Because our aim was to evaluate perfusion-related diffusion parameters, a greater number of b-values less than 200 s/mm^2 would be better at showing more subtle differences in perfusion-related parameters (PF and D*) or lack thereof. A final limitation of the study protocol could arise from injecting a constant volume of 10 mL of gadolinium contrast in patients of different weight. Some of the model-free perfusion parameters (including c_{max}, upslope, and IAUC60) could be confounded by this dose-related variability.

In conclusion, our findings show that perfusion and diffusion are both affected in cirrhosis, IVIM perfusion parameters do not correlate with DCE-MR parameters, and that the combination of diffusion and DCE-MR parameters (ADC and DV-TTP) provides excellent diagnostic performance for the detection of liver cirrhosis.

Acknowledgments

Contract grant sponsor: Radiological Society of North America; Contract grant number: RSCH 0710; Contract grant sponsor: Bracco Diagnostics Inc.

Author Manuscript Author Manuscript Author Manuscript Author Manuscript

REFERENCES

1. Afdhal NH, Nunes D. Evaluation of liver fibrosis: a concise review. Am J Gastroenterol. 2004; 99:1160–1174. [PubMed: 15180741]
2. NIH Consensus Statement on Management of Hepatitis C: 2002. NIH Consens State Sci Statements. 2002; 19:1–46.
3. Kim AI, Saab S. Treatment of hepatitis C. Am J Med. 2005; 118:808–815. [PubMed: 16084169]
4. Namimoto T, Yamashita Y, Sumi S, Tang Y, Takahashi M. Focal liver masses: characterization with diffusion-weighted echo-planar MR imaging. Radiology. 1997; 204:739–744. [PubMed: 9280252]
5. Ichikawa T, Haradome H, Hachiya J, Nitatori T, Araki T. Diffusion-weighted MR imaging with a single-shot echoplanar sequence: detection and characterization of focal hepatic lesions. AJR Am J Roentgenol. 1998; 170:397–402. [PubMed: 9456953]
6. Amano Y, Kumazaki T, Ishihara M. Single-shot diffusion-weighted echo-planar imaging of normal and cirrhotic livers using a phased-array multicoil. Acta Radiol. 1998; 39:440–442. [PubMed: 9685834]
7. Kim T, Murakami T, Takahashi S, Hori M, Tsuda K, Nakamura H. Diffusion-weighted single-shot echoplanar MR imaging for liver disease. AJR Am J Roentgenol. 1999; 173:393–398. [PubMed: 10430143]
8. Taouli B, Vilgrain V, Dumont E, Daire JL, Fan B, Menu Y. Evaluation of liver diffusion isotropy and characterization of focal hepatic lesions with two single-shot echo-planar MR imaging sequences: prospective study in 66 patients. Radiology. 2003; 226:71–78. [PubMed: 12511671]
9. Aube C, Racineux PX, Lebigot J, et al. [Diagnosis and quantification of hepatic fibrosis with diffusion weighted MR imaging: preliminary results]. J Radiol. 2004; 85:301–306. [PubMed: 15192522]
10. Koinuma M, Ohashi I, Hanafusa K, Shibuya H. Apparent diffusion coefficient measurements with diffusion-weighted magnetic resonance imaging for evaluation of hepatic fibrosis. J Magn Reson Imaging. 2005; 22:80–85. [PubMed: 15971188]
11. Lewin M, Poujol-Robert A, Boelle PY, et al. Diffusion-weighted magnetic resonance imaging for the assessment of fibrosis in chronic hepatitis C. Hepatology. 2007; 46:658–665. [PubMed: 17663420]
12. Taouli B, Tolia AJ, Losada M, et al. Diffusion-weighted MRI for quantification of liver fibrosis: preliminary experience. AJR Am J Roentgenol. 2007; 189:799–806. [PubMed: 17885048]
13. Girometti R, Furlan A, Esposito G, et al. Relevance of b-values in evaluating liver fibrosis: a study in healthy and cirrhotic subjects using two single-shot spin-echo echo-planar diffusion-weighted sequences. J Magn Reson Imaging. 2008; 28:411–419. [PubMed: 18666139]
14. Taouli B, Chouli M, Martin AJ, Qayyum A, Coakley FV, Vilgrain V. Chronic hepatitis: role of diffusion-weighted imaging and diffusion tensor imaging for the diagnosis of liver fibrosis and inflammation. J Magn Reson Imaging. 2008; 28:89–95. [PubMed: 18581382]
15. Annet L, Materne R, Danse E, Jamart J, Horsmans Y, Van Beers BE. Hepatic flow parameters measured with MR imaging and Doppler US: correlations with degree of cirrhosis and portal hypertension. Radiology. 2003; 229:409–414. [PubMed: 12970464]
16. Hagiwara M, Rusinek H, Lee VS, et al. Advanced liver fibrosis: diagnosis with 3D whole-liver perfusion MR imaging—initial experience. Radiology. 2008; 246:926–934. [PubMed: 18195377]
17. Le Bihan D, Breton E, Lallemand D, Aubin ML, Vignaud J, Laval-Jeantet M. Separation of diffusion and perfusion in intravoxel incoherent motion MR imaging. Radiology. 1988; 168:497–505. [PubMed: 3393671]
18. Le Bihan D. Intravoxel incoherent motion imaging using steady-state free precession. Magn Reson Med. 1988; 7:346–351. [PubMed: 3205150]
19. Le Bihan D, Turner R, MacFall JR. Effects of intravoxel incoherent motions (IVIM) in steady-state free precession (SSFP) imaging: application to molecular diffusion imaging. Magn Reson Med. 1989; 10:324–337. [PubMed: 2733589]
20. Le Bihan D, Turner R. Intravoxel incoherent motion imaging using spin echoes. Magn Reson Med. 1991; 19:221–227. [PubMed: 1881307]

Author Manuscript Author Manuscript Author Manuscript Author Manuscript

21. Yamada I, Aung W, Himeno Y, Nakagawa T, Shibuya H. Diffusion coefficients in abdominal organs and hepatic lesions: evaluation with intravoxel incoherent motion echo-planar MR imaging. Radiology. 1999; 210:617–623. [PubMed: 10207458]
22. Moteki T, Horikoshi H. Evaluation of hepatic lesions and hepatic parenchyma using diffusion-weighted echo-planar MR with three values of gradient b-factor. J Magn Reson Imaging. 2006; 24:637–645. [PubMed: 16888790]
23. Luciani A, Vignaud A, Cavet M, et al. Liver cirrhosis: intravoxel incoherent motion MR imaging—pilot study. Radiology. 2008; 249:891–899. [PubMed: 19011186]
24. Taouli B, Sandberg A, Stemmer A, et al. Diffusion-weighted imaging of the liver: comparison of navigator triggered and breathhold acquisitions. J Magn Reson Imaging. 2009; 30:561–568. [PubMed: 19711402]
25. Ivancevic MK, Zimine I, Foxall D, et al. Inflow effect in first-pass cardiac and renal MRI. J Magn Reson Imaging. 2003; 18:372–376. [PubMed: 12938136]
26. Gudbjartsson H, Patz S. The Rician distribution of noisy MRI data. Magn Reson Med. 1995; 34:910–914. [PubMed: 8598820]
27. Istratov AA, Vyvenko OF. Exponential analysis in physical phenomena. Rev Sci Instrum. 1999; 70:1233–1257.
28. Callot V, Bennett E, Decking UK, Balaban RS, Wen H. In vivo study of microcirculation in canine myocardium using the IVIM method. Magn Reson Med. 2003; 50:531–540. [PubMed: 12939761]
29. Yao L, Sinha U. Imaging the microcirculatory proton fraction of muscle with diffusion-weighted echo-planar imaging. Acad Radiol. 2000; 7:27–32. [PubMed: 10645455]
30. Wirestam R, Borg M, Brockstedt S, Lindgren A, Holtas S, Stahlberg F. Perfusion-related parameters in intravoxel incoherent motion MR imaging compared with CBV and CBF measured by dynamic susceptibility-contrast MR technique. Acta Radiol. 2001; 42:123–128. [PubMed: 11281143]
31. Jones RA, Easley K, Little SB, Scherz H, Kirsch AJ, Grattan-Smith JD. Dynamic contrast-enhanced MR urography in the evaluation of pediatric hydronephrosis. Part 1. Functional assessment. AJR Am J Roentgenol. 2005; 185:1598–1607. [PubMed: 16304021]
32. Bokacheva L, Rusinek H, Chen Q, et al. Quantitative determination of Gd-DTPA concentration in T1-weighted MR renography studies. Magn Reson Med. 2007; 57:1012–1018. [PubMed: 17534906]
33. Materne R, Smith AM, Peeters F, et al. Assessment of hepatic perfusion parameters with dynamic MRI. Magn Reson Med. 2002; 47:135–142. [PubMed: 11754452]
34. Dienstag JL. The role of liver biopsy in chronic hepatitis C. Hepatology. 2002; 36:S152–160. [PubMed: 12407589]
35. Maharaj B, Maharaj RJ, Leary WP, et al. Sampling variability and its influence on the diagnostic yield of percutaneous needle biopsy of the liver. Lancet. 1986; 1:523–525. [PubMed: 2869260]
36. Gronbaek K, Christensen PB, Hamilton-Dutoit S, et al. Interob-server variation in interpretation of serial liver biopsies from patients with chronic hepatitis C. J Viral Hepat. 2002; 9:443–449. [PubMed: 12431207]
37. Regev A, Berho M, Jeffers LJ, et al. Sampling error and intraob-server variation in liver biopsy in patients with chronic HCV infection. Am J Gastroenterol. 2002; 97:2614–2618. [PubMed: 12385448]
38. Ratziu V, Bonyhay L, Di Martino V, et al. Survival, liver failure, and hepatocellular carcinoma in obesity-related cryptogenic cirrhosis. Hepatology. 2002; 35:1485–1493. [PubMed: 12029634]
39. Bedossa P, Dargere D, Paradis V. Sampling variability of liver fibrosis in chronic hepatitis C. Hepatology. 2003; 38:1449–1457. [PubMed: 14647056]
40. Weigand K. Percutaneous liver biopsy: retrospective study over 15 years comparing 287 inpatients with 428 outpatients. J Gastroenterol Hepatol. 2009; 24:792–799. [PubMed: 19220661]
41. Van Beers BE, Leconte I, Materne R, Smith AM, Jamart J, Horsmans Y. Hepatic perfusion parameters in chronic liver disease: dynamic CT measurements correlated with disease severity. AJR Am J Roentgenol. 2001; 176:667–673. [PubMed: 11222202]

Author Manuscript Author Manuscript Author Manuscript Author Manuscript

42. Annet L, Peeters F, Abarca-Quinones J, Leclercq I, Moulin P, Van Beers BE. Assessment of diffusion-weighted MR imaging in liver fibrosis. J Magn Reson Imaging. 2007; 25:122–128. [PubMed: 17154179]

43. Taouli B, Martin AJ, Qayyum A, et al. Parallel imaging and diffusion tensor imaging for diffusion-weighted MRI of the liver: preliminary experience in healthy volunteers. AJR Am J Roentgenol. 2004; 183:677–680. [PubMed: 15333355]

44. Gulberg V, Haag K, Rossle M, Gerbes AL. Hepatic arterial buffer response in patients with advanced cirrhosis. Hepatology. 2002; 35:630–634. [PubMed: 11870377]

45. Le Bihan D, Turner R. The capillary network: a link between IVIM and classical perfusion. Magn Reson Med. 1992; 27:171–178. [PubMed: 1435202]

46. Henkelman RM. Does IVIM measure classical perfusion? Magn Reson Med. 1990; 16:470–475. [PubMed: 2077337]

47. Braithwaite AC, Dale BM, Boll DT, Merkle EM. Short- and mid-term reproducibility of apparent diffusion coefficient measurements at 3.0-T diffusion-weighted imaging of the abdomen. Radiology. 2009; 250:459–465. [PubMed: 19095786]

48. Koh DM, Blackledge M, Collins DJ, et al. Reproducibility and changes in the apparent diffusion coefficients of solid tumours treated with combretastatin A4 phosphate and bevacizumab in a two-centre phase I clinical trial. Eur Radiol. 2009; 19:2728–2738. [PubMed: 19547986]

49. Miyazaki K, Collins DJ, Walker-Samuel S, et al. Quantitative mapping of hepatic perfusion index using MR imaging: a potential reproducible tool for assessing tumour response to treatment with the antiangiogenic compound BIBF 1120, a potent triple angiokinase inhibitor. Eur Radiol. 2008; 18:1414–1421. [PubMed: 18351351]

Author Manuscript Author Manuscript Author Manuscript Author Manuscript

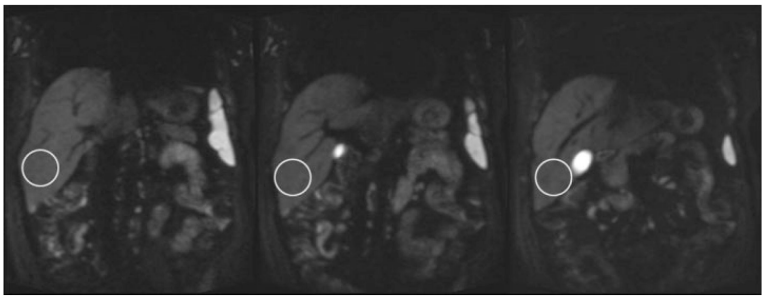

Figure 1.

ROI placement for signal intensity measurement used to quantify IVIM diffusion parameters in a 43-year-old male volunteer. Three consecutive coronal SS EPI images centered on the portal vein for b = 50 s/mm^2 are shown. ROIs are copied into the remaining images with different b-values.

Author Manuscript Author Manuscript Author Manuscript Author Manuscript

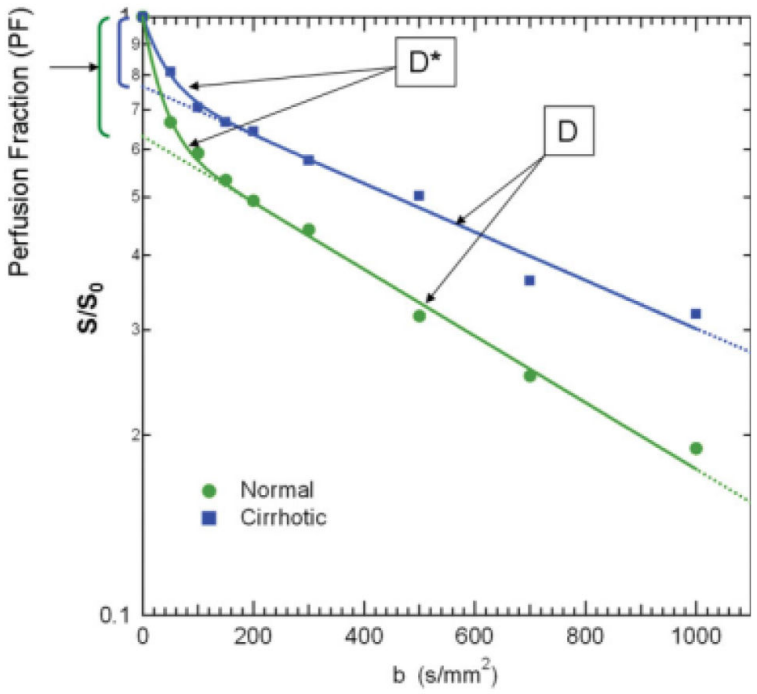

Figure 2.

IVIM diffusion decay curves shown in a 70-year-old female patient with normal liver (circles) and a 71-year-old female patient with cirrhosis related to chronic hepatitis C (squares). The same patients are shown also in Figs. 3 and 5. Y-axis: ratio of SI after application of diffusion gradient to baseline SI (in log scale) measured in liver parenchyma, x-axis: b-values (multiple b-values, 0-50-100-150-200-300-500-700-1000 s/mm^2 are used for sampling). The perfusion (or pseudodiffusion) effect is seen as an early drop in SI observed with b-values lower than 200 s/mm^2. Perfusion fraction (PF) is measured as the difference between SI for b = 0 s/mm^2 and the intercept of the high b-value monoexponential fit. D* (pseudodiffusion coefficient) measures the curvature of the initial curve. D (true diffusion coefficient) is measured with b-values higher than 200 s/mm^2. ADC was measured using all b-values with a monoexponential fit. PF (%), D* ($\times 10^{-3}$ mm^2/s), D ($\times 10^{-3}$ mm^2/s), and ADC ($\times 10^{-3}$ mm^2/s) were all decreased in the cirrhotic patient (23.52, 24.02, 0.93, 1.22 in cirrhosis vs. 36.80, 29.78, 1.28, 2.05 in normal liver, respectively). [Color figure can be viewed in the online issue, which is available at www.interscience.wiley.com.]

Author Manuscript Author Manuscript Author Manuscript Author Manuscript

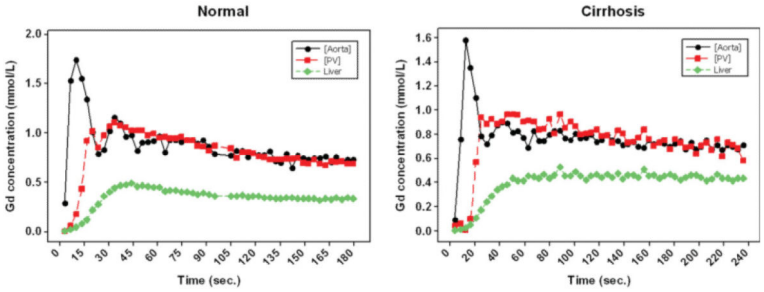

Figure 3.

Time activity curves obtained with DCE-MRI in the same patients as in Fig. 2 (curves for aorta, portal vein, and liver parenchyma are shown). TTP (sec), ART (%), DV (%), MTT (sec), and Fa (mL/100g/min) were increased in the cirrhotic liver (88.22, 44.35, 35.67, 27.22, and 34.90) compared to normal liver (42.86, 10.19, 29.16, 7.78, and 22.50). Fp (mL/100g/min), Fa + Fp (mL/100g/min) and upslope were decreased in the cirrhotic liver (43.90, 78.80, and 0.36) versus normal liver (205.80, 228.30, and 0.69). [Color figure can be viewed in the online issue, which is available at www.interscience.wiley.com.]

Author Manuscript Author Manuscript Author Manuscript Author Manuscript

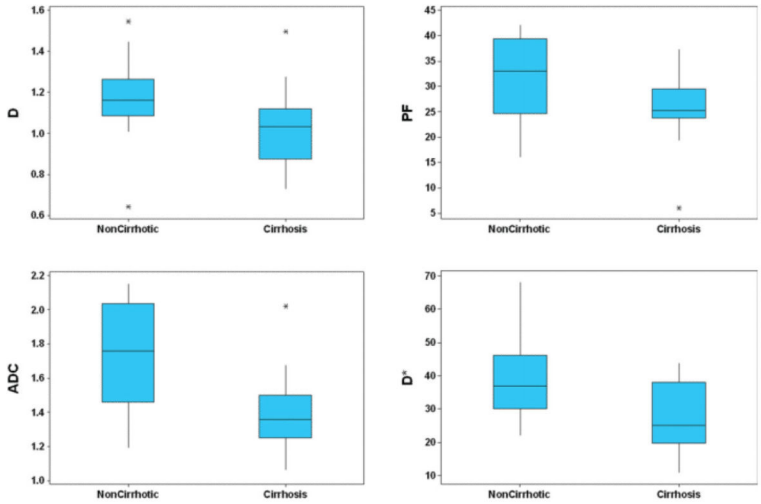

Figure 4.

Boxplot distribution of IVIM parameters in cirrhotic and noncirrhotic patients ($n = 27$). ADC showed the best discrimination. Top and bottom of boxes: 25%–75% percentiles of data, line in box: median value, *outliers. PF: perfusion fraction (%), D*: pseudodiffusion coefficient ($\times 10^{-3}$ mm^2/s), D: true diffusion coefficient ($\times 10^{-3}$ mm^2/s), ADC: apparent diffusion coefficient ($\times 10^{-3}$ mm^2/s). [Color figure can be viewed in the online issue, which is available at www.interscience.wiley.com.]

Author Manuscript Author Manuscript Author Manuscript Author Manuscript

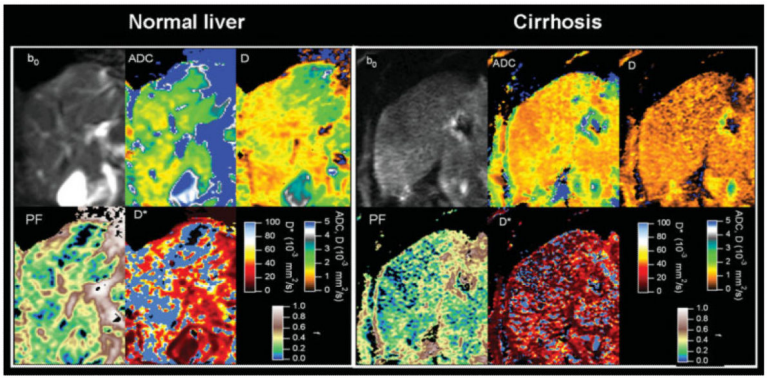

Figure 5.

Coronal voxel-based parametric maps of IVIM diffusion parameters in the same patients as in Fig. 2. The SS EPI image for b = 0 is shown for reference. ADC, D, PF, and D* maps demonstrate qualitative differences between normal and cirrhotic liver, with lower values in cirrhosis. Quantitative values for both patients are listed in Figs. 2 and 3.

Author Manuscript Author Manuscript Author Manuscript Author Manuscript

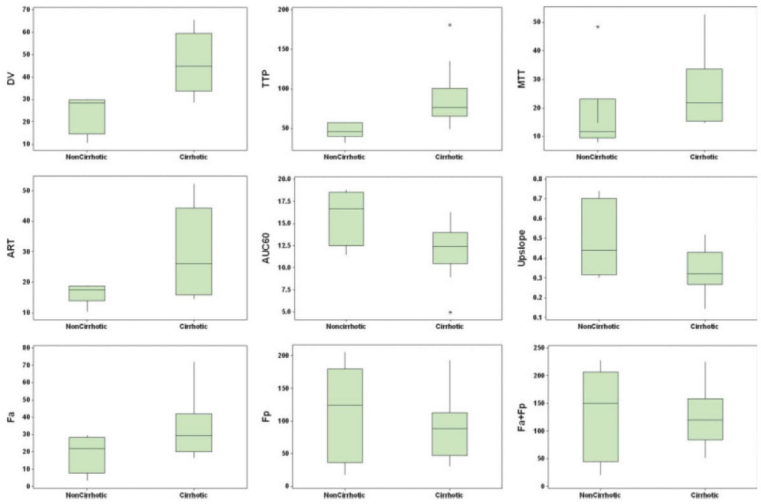

Figure 6.

Boxplot distribution of DCE-MRI parameters in cirrhotic and noncirrhotic patients (n = 20). DV (distribution volume) and TTP (time to peak) showed the best discrimination between noncirrhotic and cirrhotic patients. Top and bottom of boxes: 25%–75% percentiles of data, line in box: median value, *outliers. ART: arterial fraction (%), IAUC60: integrated area under the time activity curve over 60 s (mM.s), DV: distribution volume (%), Fa: arterial liver blood flow (ml/100g/min), Fp: portal liver blood flow (ml/100g/min), (Fa + Fp): total liver blood flow (ml/100g/min), MTT: mean transit time (sec), TTP: time to peak (sec) [Color figure can be viewed in the online issue, which is available at www.interscience.wiley.com.]

Author Manuscript Author Manuscript Author Manuscript Author Manuscript

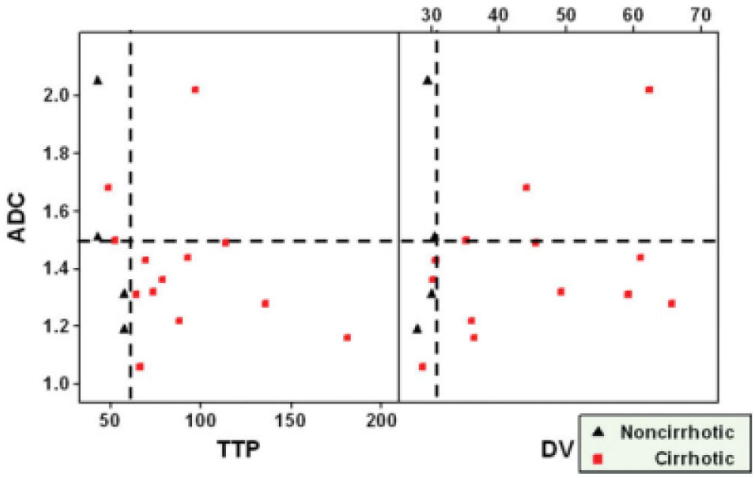

Figure 7.

Matrix plot distribution of ADC vs. TTP and DV values in 17 patients who underwent both IVIM DW- and DCE-MRI. The dashed lines indicate the threshold values calculated with logistic regression and ROC analyses (ADC ≤ 1.50×10^{-3} mm^2/s, TTP ≥57.14 sec, DV ≥30.20%). All four noncirrhotic patients had decreased TTP and DV, and 11 cirrhotic patients had decreased ADC and increased TTP or increased DV. The combination of ADC with TTP and DV provided 84.6% sensitivity (11/13), 100% specificity (4/4), 100% positive predictive value (11/11), 66.6% negative predictive value (4/6), and 88.2% (15/17) accuracy for diagnosing cirrhosis. [Color figure can be viewed in the online issue, which is available at www.interscience.wiley.com.]

Author Manuscript Author Manuscript Author Manuscript Author Manuscript

Table 1

IVIM DW- and DCE-MRI Sequence Parameters for the Different 1.5 T Systems Used (Avanto and Symphony/Sonata, Siemens Healthcare)

	Avanto (n = 21*)	Symphony/Sonata (n = 10*)
IVIM DW-MRI		
Acquisition plane	Coronal	
Acquisition scheme	PACE SS EPI	Free breathing SS EPI
TR	1 respiratory cycle	2000
TE	76	86
b-values (sec/mm^2)	0, 50, 100, 150, 200, 300, 500, 700, 1000	
EPI factor	112	192
Field of view (mm)	350-400	
Slice thickness/interslice gap (mm)/number of slices	8.0/1.6/15	
Parallel imaging factor	2	
Scan time (min)	~5	1:52
Number of averages	3	2
Acquisition matrix	192 × 192	
DCE-MRI		
Acquisition plane	Coronal	
TR	2.67	2.4
TE	0.94	0.74/0.85
Flip angle	12	
FOV Read (mm)	420	
FOV Phase (%)	100	
Slice thickness (mm)/number of slices	3/40-48	4/40-48
Parallel imaging factor	3	2
Scan time (min)	~3	~3-4
Number of averages	1	
Acquisition matrix	192 × 121	
Temporal resolution (sec)	~3.6	~4.2
Number of volumes acquired	50	50

* Four volunteers had both free breathing and PACE (PACE: prospective acquisition correction) acquisition.

Author Manuscript

Author Manuscript

Author Manuscript

Author Manuscript

Table 2

Distribution of IVIM DW-MRI Parameters in Noncirrhotic vs. Cirrhotic Group

	Non cirrhotic (n = 14)	Cirrhosis (n = 13)	p
PF (%)	32.16 ± 8.13	25.40 ± 7.48	0.0377
D* ($\times 10^{-3}$ mm^2/s)	39.61 ± 12.34	27.89 ± 10.48	0.0332
D ($\times 10^{-3}$ mm^2/s)	1.17 ± 0.21	1.04 ± 0.20	0.0377
ADC ($\times 10^{-3}$ mm^2/s)	1.73 ± 0.31	1.41 ± 0.25	0.0056

Mean ± SD are shown for each parameter.

PF: perfusion fraction, D*: pseudo-diffusion coefficient, D: true diffusion coefficient, ADC: apparent diffusion coefficient.

Author Manuscript

Author Manuscript

Author Manuscript

Author Manuscript

Table 3

Mean Coefficient of Variation (CV, in %) of IVIM Parameters Measured With Navigator Triggered (PACE: Prospective Acquisition Correction) and Free-Breathing SS EPI DW-MRI Acquisitions in five Subjects

	All (n = 5)*	PACE (n = 5)*	Free breathing (n = 4)*
PF	11.4	7.7	16.0
D*	23.8	14.6	39.1
D	5.0	3.8	6.4
ADC	3.2	3.0	3.4

*n: number of subjects (four subjects had both PACE and free breathing IVIM repeated, and one subject had only PACE IVIM DW-MRI repeated).

Author Manuscript

Author Manuscript

Author Manuscript

Author Manuscript

Table 4

Distribution of DCE-MRI Parameters in Noncirrhotic vs. Cirrhotic Group

	Noncirrhotic (*n* = 6)	Cirrhosis (*n* = 14)	*P*
TTP (sec)	46.40 ± 9.93	87.85 ± 35.51	0.0006
Upslope [mmol/(L.min)]	0.49 ± 0.20	0.33 ± 0.12	0.0913
IAUC60 (mM.s)	15.89 ± 3.24	12.14 ± 2.94	0.0791
DV (%)	23.87 ± 8.44	45.20 ± 13.03	0.0006
MTT (sec)	17.36 ± 15.38	25.11 ±11.87	0.0154
ART (%)	16.33 ± 3.29	29.99 ± 14.25	0.0913
F_a (ml/100g/min)	18.89 ± 10.60	34.12 ± 18.05	0.1253
F_p (ml/100g/min)	114.45 ± 73.11	90.73 ± 44.50	0.4442
$F_a + F_p$ (ml/100g/min)	133.34 ± 82.35	124.49 ± 48.13	0.6457

Mean ± SD are shown for each parameter, IAUC60: integrated area under the time activity curve of gadolinium contrast over 60 s from the start of contrast enhancement, ART: arterial fraction, DV: distribution volume, F_a: arterial liver blood flow, F_p: portal liver blood flow, $F_a + F_p$: total liver blood flow, MTT: mean transit time, TTP: time to peak.

Author Manuscript

Author Manuscript

Author Manuscript

Author Manuscript

Table 5

Pearson Correlation (*r*) and *P*-value for the Association of PF and D* With DCE-MRI Parameters

	PF		D*	
	r	***P***	***r***	***P***
TTP	0.01	0.9733	−0.35	0.1996
Upslope	0.06	0.8087	0.38	0.1678
IAUC60	0.07	0.7926	0.40	0.1435
ART	0.15	0.5607	−0.12	0.6740
DV	0.21	0.4222	0.27	0.3351
MTT	0.15	0.5617	0.05	0.8533
F_a	0.17	0.5173	−0.08	0.7641
F_p	0.10	0.7031	0.13	0.6396

No statistically significant correlation was observed.

PF: perfusion fraction, D*: pseudo-diffusion coefficient, TTP: time to peak, IAUC60: integrated area under the time activity curve of gadolinium contrast over 60 s from the start of contrast enhancement, ART: arterial fraction, DV: distribution volume, F_a: arterial liver blood flow, F_p: portal liver blood flow, MTT: mean transit time.

Author Manuscript

Author Manuscript

Author Manuscript

Author Manuscript

Table 6

Receiver Operating Characteristics Analysis of IVIM-DW and DCE-MR Parameters for the Diagnosis of Cirrhosis

Parameter	Az	Cutoff	Sensitivity	Specificity
IVIM				
PF (%)	0.736	≤30.01	84.6	64.2
D* ($\times 10^{-3}$ mm^2/s)	0.757	≤25.94	58.3	91.6
D ($\times 10^{-3}$ mm^2/s)	0.736	≤1.12	84.6	71.4
ADC ($\times 10^{-3}$ mm^2/s)	0.808	≤1.50	84.6	71.4
DCE-MRI				
TTP (sec.)	0.952	≥57.14	85.7	100.0
Upslope [mmol/(L.min)]	0.738	≤0.52	100.0	50.0
IAUC60 (mM.s)	0.804	≥14.69	85.7	75.0
DV (%)	0.952	≥30.20	85.7	100.0
MTT (sec.)	0.845	≥14.59	100.00	83.33
ART (%)	0.750	≥18.90	57.1	100.0
F_a (ml/100g/min)	0.720	≥29.70	50.0	100.0
F_p (ml/100g/min)	0.619	≤106.60	78.5	66.6
$F_a + F_p$ (ml/100g/min)	0.571	≤125.80	64.2	66.6

PF: perfusion fraction, D*: pseudo-diffusion coefficient, D: true diffusion coefficient, ADC: apparent diffusion coefficient, ART: arterial fraction, IAUC60: integrated area under the time activity curve of gadolinium contrast over 60 s from the start of contrast enhancement, DV: distribution volume, F_a: arterial liver blood flow, F_p: portal liver blood flow, $F_a + F_p$: total liver blood flow, MTT: mean transit time, TTP: time to peak.